Journal of Thermal Analysis, Vol. 45 (1995) 417-436

ANALYSIS OF THERMAL BEHAVIOUR OF HIGH POWER SEMICONDUCTOR LASER ARRAYS BY MEANS OF THE FINITE ELEMENT METHOD (*FEM*)

A. Bärwolff, R. Puchert, P. Enders, U. Menzel and D. Ackermann[*]

Max-Born-Institut für Nichtlineare Optik und Kurzzeitspektroskopie, Rudower Chaussee 6, D-12489 Berlin, Germany

(Received September 11, 1994)

Abstract

New results of steady-state two-dimensional finite-element computations of temperature distributions of high power semiconductor laser arrays are presented. The influence of different thermal loads on the 2*D* temperature distribution in AlGaAs/GaAs gain-guided laser arrays is investigated. The *FEM* model is tested by comparing it with analytical solutions. For numerical convenience, the latter is rewritten in a novel form, which is free of overflow problems. The maximum temperatures calculated by both methods agree within 1%. Several factors determining the thermal resistance of the device are quantitatively examined: the ratio of light emitting to non-emitting areas along the active zone, the amount of Joule losses, the current spreading, the solder thickness, and voids in the solder. This yields design rules for optimum thermal performance.

Keywords: finite element method (*FEM*), semiconductor

Introduction

High power semiconductor laser diodes [1, 2] find increasing use for pumping solid state lasers [3], material processing, and second harmonic generation [4]. The performance of such devices depends crucially on their thermal properties, which are usually characterized through the thermal resistance, R_{th}. The thermal resistance depends on the inner structure of the laser (layer thicknesses, thermal conductivities, location of heat sources) and on how the device is mounted on the heat sink (solder thickness and thermal conductivity, additional heat spreaders). Thus numerous theoretical and experimental investigations

* Now at Gesellschaft für Förderung angewandter Optik, Optoelektronik, Quantenelektronik und Spektroskopie e. V., Rudower Chaussee 5, D-12489 Berlin, Germany

0368–4466/95/ $ 4.00

John Wiley & Sons, Limited
Chichester

have been performed, in order to improve the thermal performance of such diodes [5–8] for lifetimes of 1.000 and more h.

Analytical solutions of the heat conduction equation are often impractical for modelling real devices, for instance, for complex geometric forms or when including the temperature dependence of the material parameters. Nevertheless, they are useful for testing numerical results using somewhat simplified configurations. This is the approach chosen in this paper. In particular, the layered structure of laser diodes involves drastic differences in horizontal and vertical dimensions. This poses additional difficulties to the generation of the grid for numerical computation. In particular, the trade-off between discretization error (mesh size), computing resources, and round-off error (number of elements) requires high aspect ratios of the elements, which, in turn are limited by numerical stability and accuracy.

Finite Element Modelling (*FEM*) has been proven to be a very efficient tool for the thermal analysis of semiconductor lasers [9–11]. The paper has the purpose of carrying out an appreciation of usability of the finite element method for the thermal analysis of high power lasers. To our knowledge, this is the first *FEM* 2*D* thermal model of high power laser diodes with double quantum well structure. Computing steady state 2*D* temperature distributions using the commercial *FEM* package PATRAN/P3-Thermal on a HP 705 workstation, we analyze the influence of different heat sources and their distribution and also of different solders on the thermal resistance and, thus, the temperature rise in the device under steady state condition. The device geometry and material parameters have been chosen to be typical for commercially available AlGaAs laser diodes with output powers of about 1 W.

Diode structure

We have investigated a separate confinement heterostructure with double-quantum well active zone (SCH-DQW) as sketched in Fig. 1. A multi-quantum well (*MQW*) structure with alternating content of aluminium to stop defect growth from the substrate is deposited on a GaAs substrate (layer 4). In our calculations, the thermal behaviour of this *MQW* will be simplified by collecting all thin layers into one with an aluminium content of 25% (5). The active laser part is a *DQW* with a well thickness of about 6 nm (7). The wells are embedded in layers with an aluminium content of 40% (7). Because the wells and the barrier between them are very thin, when compared with the embedding layers, we will use for them the value of the thermal conductivity of the outer layers.

The laser diode is mounted with solder (11) on a heat sink. The same solder (2) connects the contact foil (1). The metallisations of the laser contact surfaces react with both solders. It is well known, that soft solders (In, PnSn) react with the commonly used gold metallisation to intermetallic phases [12, 13], which exhibit properties very different from that of the solders. We incorporate these properties into one layer on one side of the solder and refer to them as intermet-

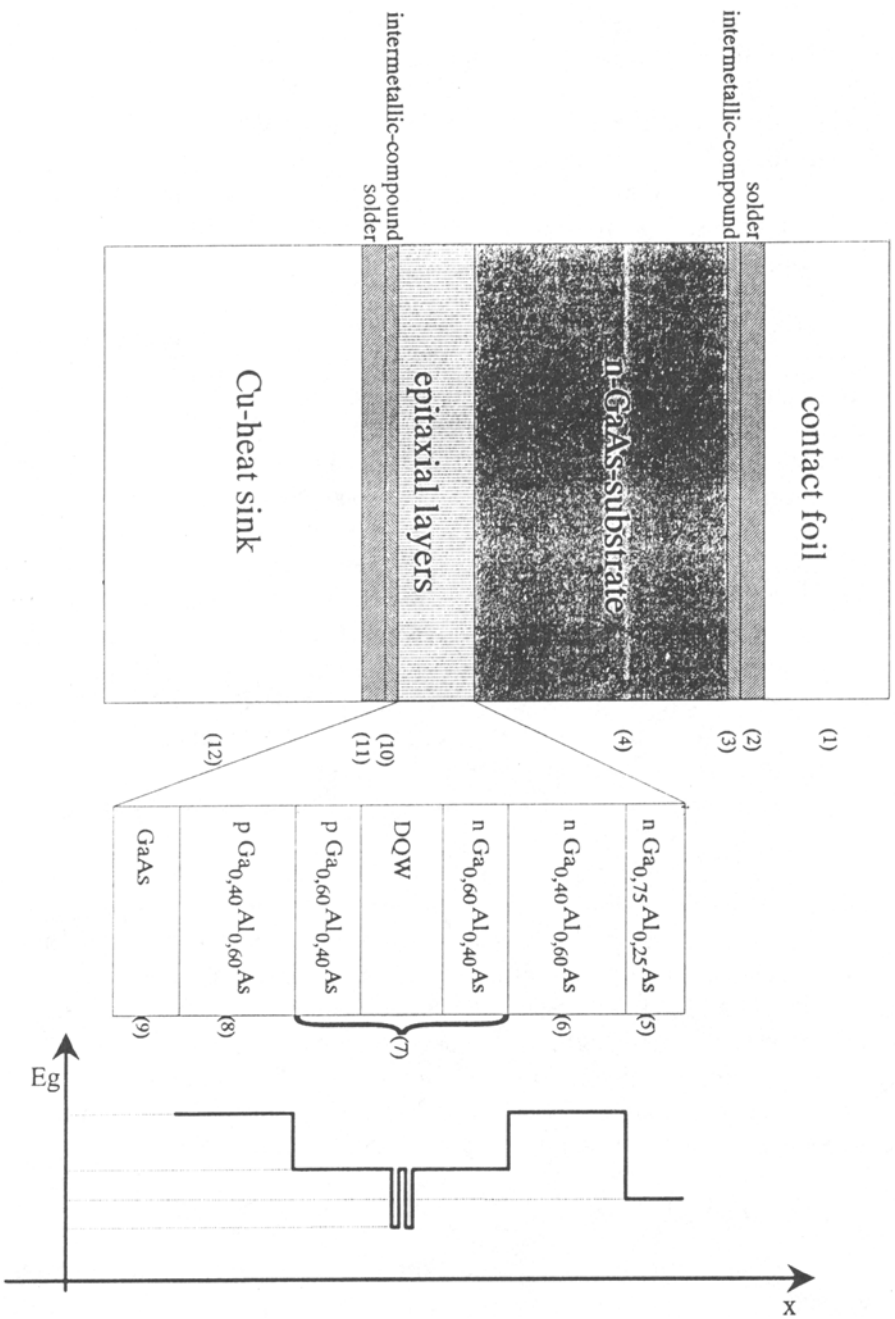

Fig. 1 Scheme of a *DQW* laser mounted on a copper heat sink with the epitaxial layers and the fundamental gap distribution showing the location of the two quantum wells

allic compound. Except computation with variation of thermal conductivities and thickness of solder we used the values listed in Table 1. The width of the laser bar is 310 μm, its resonator length equals 600 μm. The temperature of the bottom edge of the Cu-heat sink is 20°C. Heat transfer from the contact foil is due to convective cooling (convection coefficient: 25 W/m^2K).

We will vary (i), the structure parameters of the active region, such as width, package density, and power density; (ii) the Joule heat distribution in the *n*-region; (iii) the solder properties. All heat sources are assumed to be uniform within their volume of generation.

Test of the *FEM* grid by comparison with an analytical solution

The crucial step in *FEM* computations is the choice of the grid of elements. One has to find a good compromise between the discretization error, which increases with the coarseness of the grid, and the round-off error, which increases with the number of elements. Moreover, in semiconductor laser diodes, there are extremalous differences in the characteristic dimensions in horizontal (300 μm) and in vertical direction (0.2 μm). This requires a high aspect ratio of the finite elements. But this ratio is limited for numerical stability reasons. Quantum wells of thickness of about 10 nm are outside the capabilities of pres-ent-day *FEM* packages. For this reason, we average over the *DQW* part of Fig. 1.

Because of the counteraction of discretization error and round-off error, the convergence of *FEM* results with respect to some grid parameter is not necessarily a measure of accuracy. In order to get reliable results, the grid developed will be varied in size and tested by comparing *FEM* results with that of an analytical solution.

Since the critical grid region is that around the active layer, where the light emitters act as localised intense heat sources, we can facilitate this comparison by choosing a test configuration, which exhibits the most important details of the laser structures we are interested in. Thus, we take only the layers 3 to 10 and 5 emitters of Fig. 1 and neglect the Joule heating, which has little influence on the highest temperature gradients near the emitters. In what follows, we describe first the analytical solution used and then the *FEM* computation together with the numerical results. The analytical solution is described in some detail, because we chose a non-standard ansatz for the temperature function.

The analytical model

The stationary heat conduction equation for the 2*D* temperature distribution $T(x,y)$ reads

$$\nabla(\lambda(y)\cdot\nabla T(x, y)) + Q(x, y) = 0 \qquad (1)$$

$\lambda(y)$ – thermal conductivity, dependent on the layer; $Q(x, y)$ – power per unit volume of the heat sources. The boundary conditions are: ideal heat sink at p-contact ($y=0$), adiabatic ones at the two side faces ($x = b/2$ and $x = -b/2$), and convective cooling at the top surface ($y = h$). This means

$$T(x, 0) = 0 \tag{2a}$$

$$-\lambda_N \cdot \frac{d}{dy} T(x, h) = \alpha \cdot T(x, h) \tag{2b}$$

$$\frac{\partial}{\partial x} T\left(-\frac{b}{2}, y\right) = \frac{\partial}{\partial x} T\left(\frac{b}{2}, y\right) = 0 \tag{2c}$$

where λ_i is the thermal conductivity of the i-th layer ($i=1...N$), N the number of layers, and b the width of the stack. We will solve Eq. (1) by means of Green's functions, e.g. [14, 15]. First, the homogeneous problem, $Q=0$, is solved. Due to the rectangular geometry of the stack, it is separable as

$$T(x, y) = X(x) \cdot Y(y) \tag{3}$$

Inserting into (1) and dividing by (λXY) yields

$$\frac{1}{\lambda(y) \cdot Y(y)} \cdot \frac{d}{dy}\left(\lambda(y) \frac{d}{dy} Y(y)\right) = -\frac{1}{X(x)} \cdot \frac{d^2}{dx^2} X(x) = \mu^2 \tag{4}$$

where μ is the separation constant. By virtue of the boundary conditions (2c), one obtains the spatial diffusion modes in x-direction, $X_k(x)$ (k–numbering index and wave number of mode k) as

$$X_k(x) = \cos(\mu_k x); \quad k = 0, 1, 2, \ldots \infty \tag{5}$$

(not normalised). The odd modes have been omitted, because the sources are symmetric, $Q(-x, y) = Q(x, y)$, see below. For the function $Y(y)$, Eq. (4) yields

$$\frac{d}{dy}\left(\lambda(y) \frac{dY(y)_k}{dy}\right) = (\mu_k)^2 \lambda(y) \cdot Y(y)_k \tag{6}$$

Because of the jumps in the thermal conductivity, $\lambda(y)$, at the layer interfaces, Eq. (6) is solved within each layer, i, $i=1..N$, and then, these layer solutions are matched by requiring continuity of temperature and heat current density at all N-1 layer interfaces

$$Y(h_i - 0)_k = Y(h_i + 0)_k \tag{7a}$$

$$\lambda_i \cdot \frac{d}{dy} Y(h_i - 0)_k = \lambda_{i+1} \cdot \frac{d}{dy} Y(h_i + 0)_k \qquad i = 1, 2, \ldots, N-1 \qquad (7b)$$

$$h_o = 0; \quad h_i = \sum_{j=1}^{i} d_j \qquad i = 1, 2, \ldots, N \qquad (8)$$

where d_i is the thickness of the i-th layer. Now, Eq. (6) is not an eigenvalue equation, because μ_K has been fixed already. Thus, one deals with two sets of solutions, one, say, $Y_o(y)$, fulfilling the boundary condition (2a), the other one, $Y_h(y)$ – condition (2b). In order to avoid numerical overflow, we make different ansatzes for them and do not use the standard hyperbolic functions. Within the i-th layer,

$$Y_o(y)_{i,o} = A_{o_{i,o}} + B_{o_{i,o}} \cdot \frac{y - h_{i-1}}{d_i} \qquad (k = 0)$$

$$h_{i-1} \le x \le h_i \qquad (9a)$$

$$Y_o(y)_{i,k} = A_{o_{i,k}} \cdot e^{\mu_k y} + B_{o_{i,k}} \cdot e^{\mu_k (2 \cdot h_{i-1} - y)} \qquad (k > 0)$$

and

$$Y_h(y)_{i,o} = A_{h_{i,o}} + B_{h_{i,o}} \cdot \frac{y - h_i}{d_i} \qquad (k = 0)$$

$$h_{i-1} \le x \le h_i \qquad (9b)$$

$$Y_h(y)_{i,k} = A_{h_{i,k}} \cdot e^{\mu_k (y - 2 \cdot h_i)} + B_{h_{i,k}} \cdot e^{-\mu_k \cdot y} \qquad (k > 0)$$

For simplicity, we have singled out the case $k = 0$ and chosen the coefficients for $k = 0$ independently of those for $k \neq 0$, i.e., $A_{o;i,o} \neq \lim_{k \to o} A_{o;i,k}$ etc.! Without loss of generality, we choose

$$A_{o_{1,k}} = 1 \qquad B_{o_{1,k}} = -1 \qquad A_{h_{N,k}} = 1 \qquad (10a)$$

$$B_{h_{N,o}} = \frac{-\alpha \cdot d_N}{\lambda_N} \quad (k = 0) \qquad B_{h_{N,k}} = \frac{\lambda_N + \frac{\alpha}{\mu_k}}{\lambda_N - \frac{\alpha}{\mu_k}} \quad (k > 0) \qquad (10b)$$

From Eq. (7) one obtains the interlayer transfers of the coefficients A and B as

$$i = 2, 3, \ldots N: \quad A_{o_{i,o}} = A_{o_{i-1,o}} + B_{o_{i-1,o}}; \quad B_{o_{i,o}} = \frac{\lambda_{i-1} d_i}{d_{i-1} \cdot \lambda_i} \cdot B_{o_{i-1,o}} \quad (k = 0) \tag{11a}$$

$$\begin{pmatrix} A_{o_{i,k}} \\ B_{o_{i,k}} \end{pmatrix} = \begin{bmatrix} \frac{1}{2} \cdot \left(1 + \frac{\lambda_{i-1}}{\lambda_i}\right) & \frac{M_{i-1,k}}{2} \cdot \left(1 - \frac{\lambda_{i-1}}{\lambda_i}\right) \\ \frac{1}{2} \cdot \left(1 - \frac{\lambda_{i-1}}{\lambda_i}\right) & \frac{M_{i-1,k}}{2} \cdot \left(1 + \frac{\lambda_{i-1}}{\lambda_i}\right) \end{bmatrix} \cdot \begin{pmatrix} A_{o_{i-1,k}} \\ B_{o_{i-1,k}} \end{pmatrix} \quad (k > 0) \tag{11b}$$

$$M_{i-1,k} = \exp(-2\mu_k \cdot d_i); \quad i = 1, 2, \ldots, N; \quad (k > 0) \tag{11c}$$

$$i = N, N-1, \ldots 2: \quad A_{h_{i-1,o}} = A_{h_{i,o}} - B \quad B_{h_{i-1,o}} = \frac{\lambda_i \cdot d_{i-1}}{\lambda_{i-1} \cdot d_i} \cdot B_{h_{i,o}} \quad (k = 0) \tag{11d}$$

$$\begin{pmatrix} A_{h_{i-1,k}} \\ B_{h_{i-1,k}} \end{pmatrix} = \begin{bmatrix} \frac{M_{i,k}}{2} \cdot \left(1 + \frac{\lambda_i}{\lambda_{i-1}}\right) & \frac{1}{2} \cdot \left(1 - \frac{\lambda_i}{\lambda_{i-1}}\right) \\ \frac{M_{i,k}}{2} \cdot \left(1 - \frac{\lambda_i}{\lambda_{i-1}}\right) & \frac{1}{2} \cdot \left(1 + \frac{\lambda_i}{\lambda_{i-1}}\right) \end{bmatrix} \cdot \begin{pmatrix} A_{h_{i,k}} \\ B_{h_{i,k}} \end{pmatrix} \quad (k > 0) \tag{11e}$$

$M_{i,k}$ are auxiliary coefficients.

The two solutions of the homogeneous problem yield the solution of the inhomogeneous Eq. (1) as

$$T(x,y) = \sum_{k=0}^{\infty} X(x)_k \cdot \left(Y_h(y)_k \cdot \int_0^y \frac{Y_o(y')_k \cdot q(y')_k}{W(y')_k \cdot \lambda(y')} dy' + Y_o(y)_k \cdot \int_y^h \frac{Y_h(y')_k \cdot q(y')_k}{W(y')_k \cdot \lambda(y')} dy' \right) \tag{12}$$

Here

$$W(y)_k = Y_o(y) \cdot \frac{d}{dy} Y_h(y)_k - Y_h(y) \cdot \frac{d}{dy} Y_o(y)_k = W_{i,k} \quad h_{i-1} \le y \le h_i \tag{13a}$$

$$W_{i,o} = \frac{1}{d_1} \cdot (B_{h_{i,o}} \cdot A_{o_{i,o}} - B_{o_{i,o}} \cdot A_{h_{i,o}} + B_{h_{i,o}} \cdot B_{o_{i,o}}) \quad (k = 0) \tag{13b}$$

$$W_{i,k} = 2 \cdot \mu_k \cdot (-A_{o_{i,k}} \cdot B_{h_{i,k}} + B_{o_{i,k}} \cdot A_{h_{i,k}} \cdot M_{i,k}) \quad (k > 0) \tag{13c}$$

is the Wronskian of the fundamental system $\{Y_o, Y_h\}$. Further,

$$q(y)_k = \int_{-\frac{b}{2}}^{\frac{b}{2}} \frac{Q(x,\, y)\cdot X(x)_k}{||X(x)_k||^2}\, dx \qquad ||X(x)_k||^2 = \int_{-\frac{b}{2}}^{\frac{b}{2}} X(x)_k^2 dy = \begin{Bmatrix} b & \text{for } k = 0 \\ \frac{b}{2} & \text{for } k > 0 \end{Bmatrix} \quad (14a)$$

is the mode expansion (Fourier transform w.r.t. the function system $\{X_k\}$) of the source function $Q(x,y)$. We assume, that the heat source of power P_v be localized in 5 stripes along the active zone (cf. Fig. 1), and obtain

$$q(y)_k = q_k \cdot Q_y(y) \cdot Q_o \quad (14b)$$

$$q_o = \frac{5 \cdot w}{b} \qquad (k > 0) \quad (14c)$$

$$Q_o = \frac{P_v}{L \cdot 5 \cdot w \cdot d_5} \quad (15a)$$

$$Q_y(y) = \begin{Bmatrix} 1 & \text{for } y \in \text{ active layer} \\ 0 & \text{otherwise} \end{Bmatrix} \quad (15b)$$

Here, $b_o = 3$ µm is the distance between the first emitter and the side wall, $w = 4$ µm the width of the single emitter, and $b_p = 10$ µm the period of the array.

In this form, the analytical solution can be calculated with an arbitrary number of terms in the sum of formula (14), since there are no factors of the form $e^{+\mu y}$. It will be used as – measure for the accuracy of the *FEM* results, see Fig. 2 below.

FEM grid and test computations

For the computation of the 2*D* temperature distribution, the geometrical model shown in Fig. 1 is subdivided into 26970 finite elements with 174 regions. Except the variation of the mesh size the smallest and the biggest element being of the size 0.2×2 µm^2 and 6.4×2 µm^2, respectively. Due to symmetry, only a half of the structure may be computed, in order to reduce model size and CPU time.

For the comparison with the analytical solution, we have used the same simplified model as in section 3.1. To get a global survey, Fig. 2 displays the corresponding 2*D* temperature distribution of a 5-stripe laser array. The analytical and the finite element method yield the characteristic isotherms. Minor deviations between them are caused by the finite element size and node location, the

resolution of the drawing routines, and, of course, by the differences resulting from the computation procedure. The temperature rise is only small (about 2.6°C) for the shown detail of the whole structure.

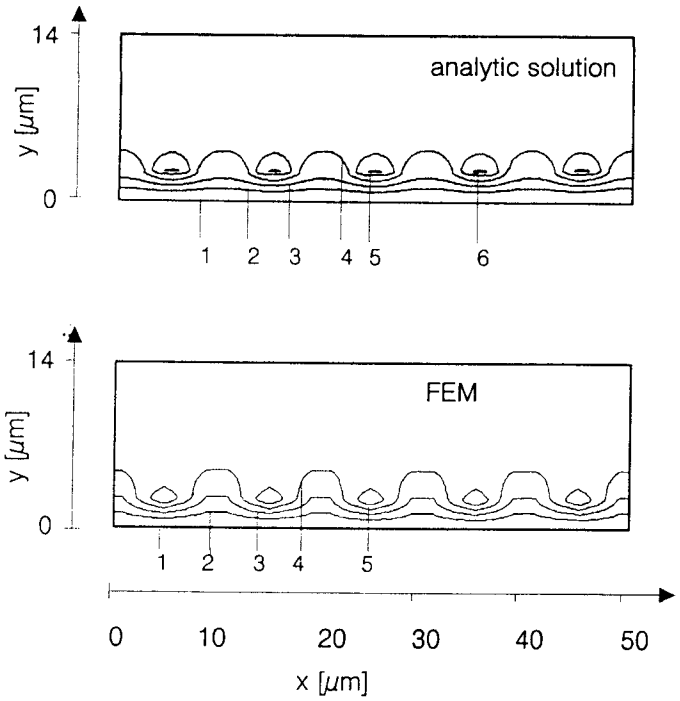

Fig. 2 Temperature distribution in a laser array calculated by (a) analytically and (b) numerically (*FEM*) solving the heat equation. The vertical structure is that of Fig. 1. Shown are the details near 5 emitting stripes. The heat power is 70 mW per stripe located at the *p–n* junction, the Joule heat has been neglected. Isotherm's on a vertical section in the middle of the device. Their values are: 1 - 20°C (heat sink temperature); 2 - 20.5°C; 3 - 21°C; 4 - 21.5°C; 5 - 22°C; 6 - 22.5°C

A more quantitative comparison between both methods is provided in Fig. 3 showing the lateral temperature distribution on the top of the active region. The resolution of the *FEM* curve is determined by the horizontal element length of 2 μm (the temperature is evaluated only at the corners of the elements). The overall agreement between the *FEM* and the analytical results is very good. The maximum temperature for the analytical solution and the *FEM* are 22.543 and 22.574°C, respectively. The difference between temperature maxima computed by *FEM* and analytical solution differ by about 1% of the total temperature rise. This is less than the accuracy of the known values of the material parameters. The good agreement between the analytical and the *FEM* results gives confidence in the correctness of this *FEM* grid. The following tests will, thus, be related to the results for this grid.

As noted above, the element size can considerably influence the result. Laser diodes exhibit inner structures with aspect ratios as high as 300 μm lateral device width to 6 nm quantum well thickness (cf. Fig. 1), for instance. It is not possible to work here with elements of the size of the smallest vertical dimen-

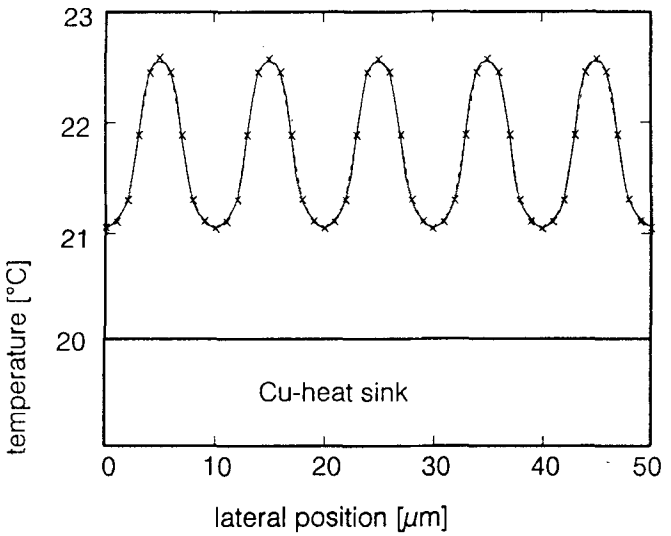

Fig. 3 Lateral temperature distribution on the top of the active region (interface between layers 6 and 7). Heat dissipation as in Fig. 2 solid curve and horizontal line – analytical solution and its mean value (k=0 term in formula (14)); crosses - *FEM* results. The *FEM* values are close to the analytical ones

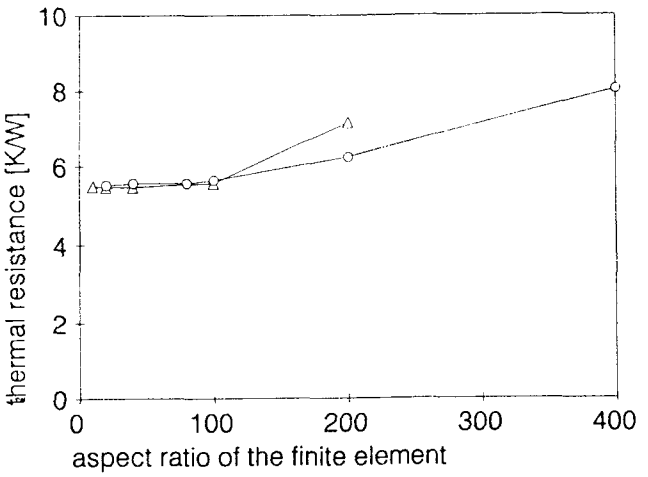

Fig. 4 Thermal resistance of a 20-stripe array with the vertical structure of Fig. 1 as function of the aspect ratio the finite element size for lateral element dimensions of 2 μm (Δ) and 4 μm (o), respectively

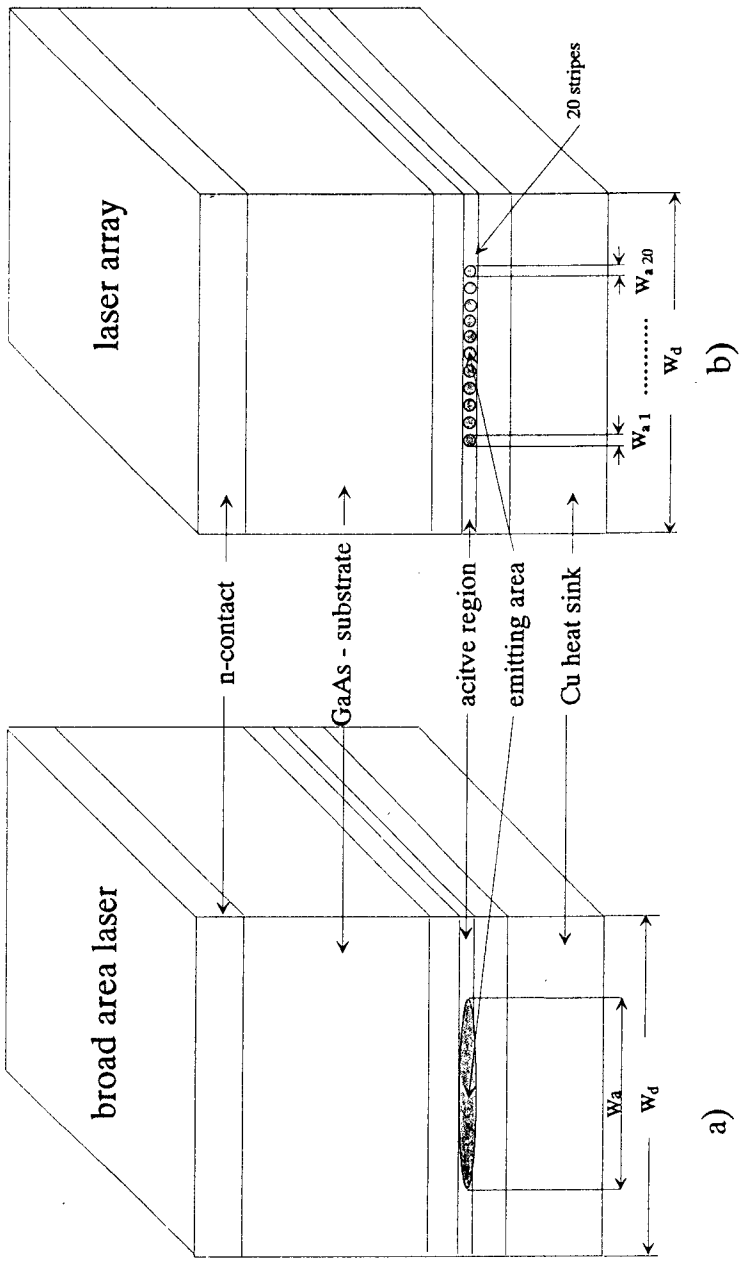

Fig. 5 Scheme of a broad area laser (a) and a laser array with the emitting regions (b). The inner structure is the same as in Fig. 1

sion, because the number of elements (about $2 \cdot 10^9$ with 6×6 nm^2) and the round-off error are too high for computation. Hence, for the modelling of such structures, it is necessary to use elements with aspect ratios as large as possible. For numerical reasons, however, the aspect ratio of the finite elements is principally limited, although this limit depends on the problem under consideration. For this, we have varied the vertical element length between 0.01 μm and 0.2 μm for lateral element lengths of 2 μm and 4 μm, see Fig. 4. Taken the result for on aspect ratio of 10 as measure, the numerical error is negligible up to the aspect ratio of 100 for 4 μm lateral extension and for 2 μm lateral extension, respectively. We conclude, that if one models such structures with this numerical package, aspect ratios as large as 100 yields additional errors of a few percents only.

Influence of various structure parameters on the thermal resistance

For characterising the influence of different diode and mounting parameters on the thermal performance, we use the thermal resistance, R_{th}. We define the thermal resistance as the ratio of the maximum local temperature rise in the device, ΔT_{max}, and the total power loss, P_{loss}, which is the difference between the total electrical power consumed by the laser, P_{tot}, and the optical output power, P_{opt},

$$R_{th} = \frac{\Delta T_{max}}{P_{loss}} = \frac{\Delta T_{max}}{P_{tot} - P_{opt}} \tag{16}$$

Some authors prefer the ratio of the maximum temperature and the total power, $\Delta T_{max}/P_{tot}$, e.g. [11]. Below lasing threshold ($P_{opt} \approx 0$) both definitions are equivalent. Above lasing threshold, however, the latter yields an artificial decrease of the thermal resistance. In what follows, we examine the influence of various structure parameters on the thermal resistance (16) using the *FEM* model described above.

Variation of the package density

By virtue of two-dimensional heat spreading, the thermal resistance depends on the extension of the emitting regions. For broad-area lasers (Fig. 5), the characteristic parameter is the package density:

$$D_P = \frac{w_a}{w_d} \tag{17}$$

The thermal resistance is minimum, when the heat source extends over the whole stack width ($D_p = 100\%$) and rises with increasing concentration of the

heat dissipation (decreasing D_p), as seen in Fig. 6 (in order to separate the individual effects, Joule heating is neglected here). For package densities lower than 40% changes of the emitter width are of much more influence, than for larger package densities. The heatflow to the Cu-heat sink is most efficient when the heat source, i.e. the active region, covers the total cross section of the heat sink. Consequently, decreasing the package density is equivalent to a smaller area available for heat transfer and leads to an increase of R_{th}.

In a multi-stripe laser array, the thermal resistance depends on the width of the single emitters and on the space between them; the package density (17) ($w_a = \Sigma w_{ai}$) becomes higher with higher stripe width and influences the thermal resistance. Figure 7 displays these relationships for the array of Fig. 5. Note, that the variation of the distances between the stripes does not change the package density. If the distance between the emitters becomes small the thermal resistance rises up to the case of broad area lasers with the same package density as the stripe laser array. The curves show that the thermal resistance is the less, the more the heat sources are distributed over a large area. This is clearly an effect of the heat current spreading.

The results suggest that a wide emitting region is favourable for effective cooling. On the other hand, wide emitters tend to inhomogenous near field patterns due to the excitation of higher-order lateral resonator modes. This leads to local power density peaks, which in turn are to be avoided. Hence, the optimum package density is some compromise between the requirements for heat removal and resonator size.

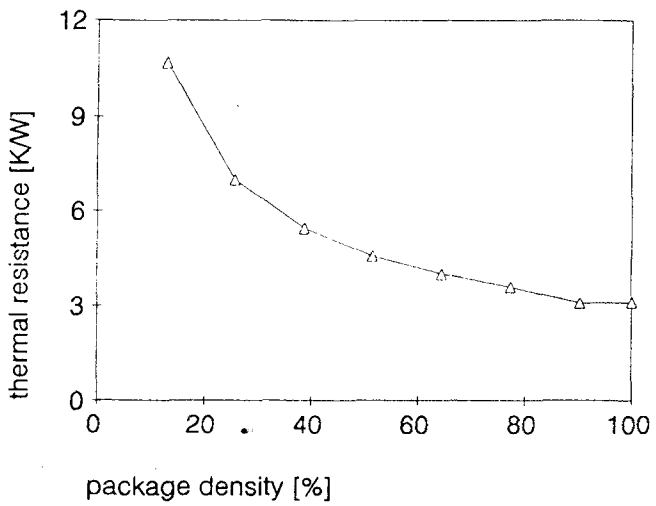

Fig. 6 Dependence of the thermal resistance on the package density for the broad area laser of Fig. 5a

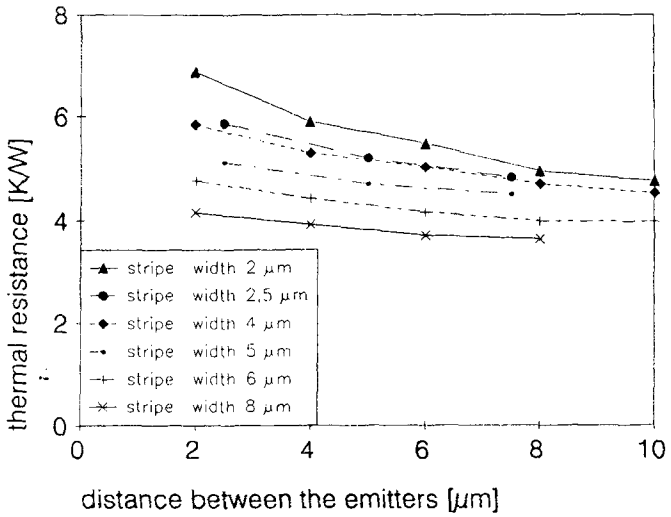

Fig. 7 Dependence of the thermal resistance on the distance between the emitters for different stripe widths in the laser array of Fig. 5b

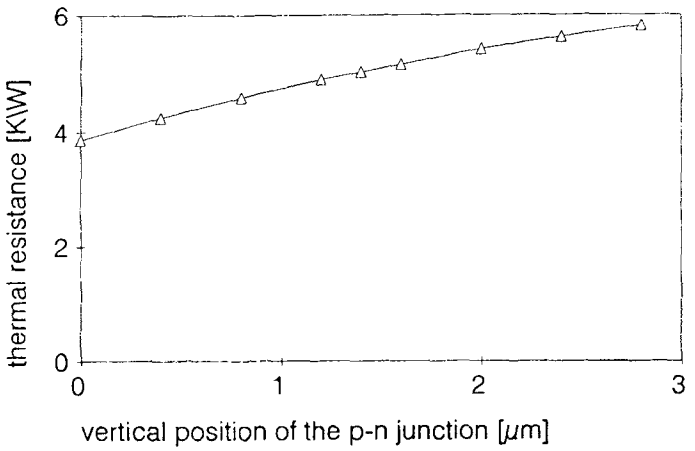

Fig. 8 Dependence of the thermal resistance on the vertical position of the *p–n* junction as heat source. The location varies from the interface to layer 8 (0 μm) to the interface to layer 6 (3 μm)

Another important factor is the distance between the emitters and the heat sink, in particular, as the thermal conductivity of GaAlAs is rather poor, when compared with that of GaAs (Table 1). Consequently, for a small thermal resistance, the GaAlAs layers should be as thin as possible. On the other hand, their thickness' have an essential influence on the optical and the electrical properties of the laser. We have changed the location of the active region relative to the

Table 1 Thickness and heat conductivity of the individual layers of Fig. 1

Layer	Thermal conductivity / $W \cdot m^{-1} \cdot K^{-1}$	Thickness / μm
1	384	48
2	87	9.4
3	200	0.2
4	44	90
5	13	0.4
6	11.4	0.6
7	11	3
8	11.4	0.6
9	44	0.2
10	200	0.2
11	87	2
12	384	150

heat sink by shifting it vertically within the embedding $Ga_{0.6}As_{0.4}As$-layer (layer 7 in Fig. 1). The results are shown in Fig. 8. A shift of 3 μm implies a change of the thermal resistance of about 2 K/W. This finding illustrates that the control of the location of the *p–n*-junction is quite important for the thermal performance.

Joule heating; variation of the current spreading

In the computations above (Figs 6, 7, 8) the Joule heating has not been included, i.e., the heat was assumed to be generated only in the active region. However, as the amount of Joule heating increases with the pump current, it is expected to play an important role in high-power laser diodes. For the temperature of the active region, the current spreading in the *n*-region seems to be important. Actually, the knowledge of the current density distribution requires the solution of the Poisson equation. For this, simplifying analytical expressions have been reported [9]. In order to get an impression for the accuracy being necessary for a reliant description of this effect, we have investigated the two extremalous cases, viz., (I) immediate complete spreading and (II) no spreading at all. The results are shown in Fig. 9.

Surprisingly, the current distribution appears to exhibit a very small influence on the thermal resistance. It is somewhat larger in the case of broad area lasers, but this difference is not very significant. We assume, that most of this heat current spreads already in the substrate and then flows quasi-one-dimensionally through the *p*-region. Consequently, the *p*-regions build for it a smaller

thermal resistance, than for the heat current from the emitters. As a consequence, its effect on the maximum temperature in the emitting regions is less pronounced. Sarzala & Nakwaski [11] have obtained much larger differences, but in their oxide-stripe structure, the heat is forced to flow mainly through the small contact below the emitter, such that the heat spreading effect is much smaller.

Varying the mounting

The solder has two functions. First, it provides the mechanical, electrical, and thermal contact of the laser diode to the heat sink and to the contact foil.

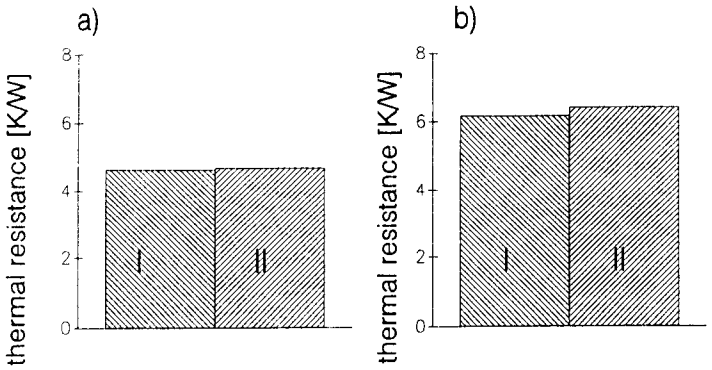

Fig. 9 Influence of the current spreading on the thermal resistance. (a) laser array with 20 stripes of 4 μm width each; (b) broad area laser, emitter width 80 μm. I - immediate complete spreading; II - no spreading

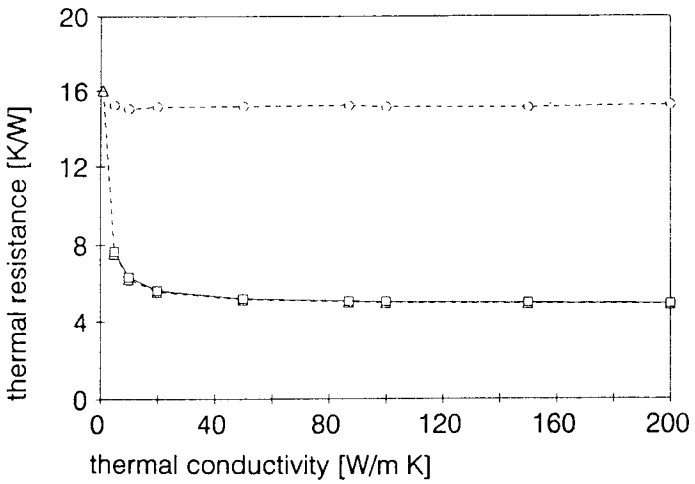

Fig. 10 Thermal resistance as function of the thermal conductivity of the solder to the copper heat sink (solder 1) and to the contact foil (solder 2), respectively. Δ – uniform variation of both solders; o – variation of solder 2 with $\lambda_{solder\,1} = 1\ W \cdot m^{-1} \cdot K^{-1}$; □ – variation of solder 1 with $\lambda_{solder\,2} = 1\ W \cdot m^{-1} \cdot K^{-1}$

These functions are best fulfilled by a thin film of soldering material. Second, it has to compensate the very different thermal expansion coefficients of the copper heat sink and the semiconductor material [16]. Here, a thicker layer is favourable. In practice, one has to find a compromise between both requirements.

In this work, we have varied the thickness' and the thermal conductivities of the soldering layers in Fig. 1. Figure 10 illustrates the influence of their thermal conductivities on the thermal resistance. Obviously, the thermal properties of the soldering layer to the contact foil have a negligible effect. This is due to the small amount of cooling through the upper contact by convective cooling. On the contrary, the thermal properties of the soldering layer to the heat sink are quite important for the thermal resistance. Thus, this solder should have a very high thermal conductivity (>44 W/m K). However, in order to reduce thermal stresses, soft solders are used, which exhibit only mediocre values of thermal conductivity. If this value is less than that of GaAs (44 W/m K), the solder thickness is significant for the thermal resistance, and heat flow through the substrate becomes more important. In turn, if the thermal conductivity of the solder is comparable with or higher than 44 W/m K, the solder thickness is of less influence.

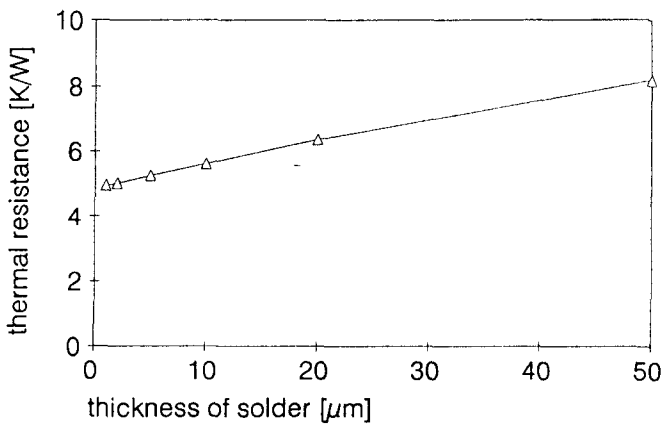

Fig. 11 Thermal resistance as function of the thickness of the solder between the copper heat sink and the laser array (layer 2 in Fig. 1)

Thus, we have examined the thermal resistance as a function of this thickness, see Fig. 11. Obviously, the dependence is almost linear. This means, that the heat flow through this layer is nearly quasi-one-dimensional. For such cases, the contribution of the soldering layer to the thermal resistance equals simply $R_{\text{th, solder}}=d_{\text{solder}}/A\lambda_{\text{solder}}$, where A is the cross section for the heat flow through this layer.

Real solder layers are not homogeneous, but contain a number of voids such as inclusions of air, clean-up agents or fluxes and areas which do not wet during welding process. This decreases the cross section for the heat flux, because the thermal conductivity of air equals only $25 \cdot 10^{-3}$ W/m K [17]. We have considered two cases, (i), there are small voids uniformly distributed, (ii), one large void in the middle of the solder layer, see Fig. 12.

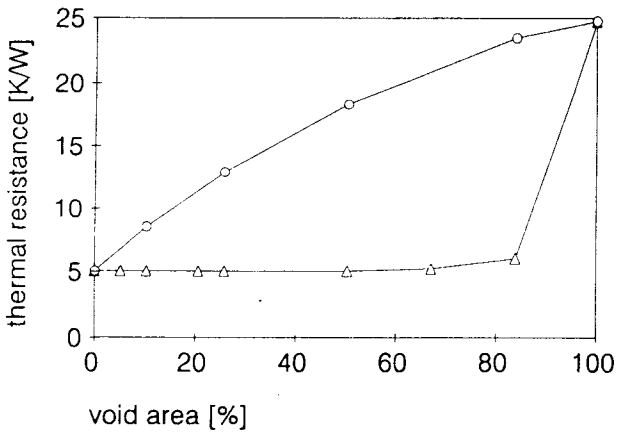

Fig. 12 Influence of voids on the thermal resistance of laser arrays. Δ - uniform distribution of small voids of the size of 2 μm×0.2 μm; o - one large void of thickness 0.2 μm extending laterally from the middle of the solder layer

Due to the heat spreading and the high thermal conductivity of the solder modelled, the small voids have little influence on the thermal resistance, as long as the remaining cross section is large enough. This is in good agreement with the dates by Yerman [17] for a high power transistor. In contrast, a larger void blocks much more the direct heat flow from the (inner) emitters to the heat sink and, consequently, leads to a significant rise of the thermal resistance already for small void areas. These results stress the relevance of the solder properties and of the welding process for the thermal device performance. It shows that not only the thermal resistance has importance on the choice of solder for welding of high power lasers.

Conclusions

We have investigated the steady-state thermal properties of *DQW* SCH GaAlAs high power laser arrays by means of two-dimensional finite-element computations. Special attention has been devoted to the optimisation of the *FEM* grid. For testing a basic *FEM* grid, we have developed an analytical solution of the heat equation, which is free of overflow problems in computing the Fourier

series for the temperature distribution (the simpler formulae of Joyce and Dixon [14] are applicable only for infinitely thin heat sources and on the line of these sources). For this grid, the *FEM* results compare well with the analytical ones.

We have studied the influence of various structural and material parameters on the thermal resistance of high power laser diodes using a simplified model of a typical commercial device. We believe, that it is more appropriate to relate the thermal resistance to the power loss, rather than to the total power, for, in the latter case, its behaviour would suddenly change at the lasing threshold.

Heat spreading has a significant influence on the thermal resistance, for, the more the heat spreads, the more the heat flow cross section increases. Among others, it determines the influence of the package density and of voids in the solder on the thermal resistance. It may also be responsible for that the electrical current spreading in the *n*-region has only a minor effect on the temperature in the active region.

In summary, we have obtained several design rules for optimum thermal performance. Maximum heat removal is achieved, when

- the emitting regions are laterally extended;
- the *p–n* junction is located closely to the heat sink;
- the soldering layer to the heat sink is thin and of high thermal conductivity;
- there are at most few small voids in the solder.

The solder to the contact foil and, for fixed series resistance, the current spreading on the *n*-side have little influence on the thermal resistance. Unfortunately, some of these rules contradict to other requirements, such as mechanical stress reduction and maximum optical and electrical confinement in the active region. In practice, appropriate compromises have to be found.

* * *

The authors would like to thank Prof. T. Elsässer for helpful discussion. This work has been supported by the Bundesministerium für Forschung und Technologie (BMFT) under the contract number 13N6016.

References

1 J. G. Endriz, M. Vakili, G. S. Bowder, M. De Vito, J. M. Haden, G. L. Harnagel, W. E. Plano, M. Sakamoto, D. F. Welch, St. Willing, D. P. Vorland and H. C. Yao, IEEE J. Quantum Electron. QE-28 (1992) 952.
2 M. Sakamoto, J. G. Endriz and D. R. Scifres, Electron. Lett., 28 (1989) 178.
3 D. Golla, A. Bernd, W. Schöne, I. Kröpke and H. Schmidt, Laser und Optoelektronik, 25 (1993) 61.
4 A. Hayes, L. Marschall, R. Burnham, Advanced Solid State Lasers, Vol. 10, OSA Proceedings Series 1991, p. 255.
5 J. S. Yoo, S. Fang and H. H. Lee, J. Appl. Phys., 74 (1993) 6503.
6 H. I. Abdelkader, H. H. Hausien and J. D. Martin, Rev. Sci. Instrum., 63 (1992) 2004.

7 H. H. Lee, IEEE J Quantum Electron. QE-29 (1993) 2619.
8 F. P. Dabkovski, A. I. Chin, P. Gavrilowic, S. Alie and D. M. Beyea, Appl. Phys. Lett., 64 (1994) 13.
9 R. P. Sarzala and W. Nakwaski, J. Thermal Anal., 36 (1990) 1171.
10 R. P. Sarzala and W. Nakwaski, J. Thermal Anal., 36 (1993) 1297.
11 R. P. Sarzala and W. Nakwaski, Opt. Quantum Electron., 26 (1994) 87.
12 G. Matijasevic and C. C. Lee, J. Electron. Mat., 18 (1989) 327.
13 C. C. Lee, C. Y. Wang and G. S. Matijasevic, IEEE Trans. Comp., Hybrids, Manuf. Technol., 14 (1991) 407.
14 W. B. Joyce, R. W. Dixon, J. Appl. Phys., 46 (1975) 855.
15 H. J. Dirschmidt, W. Kummer and M. Schweda, Einführung in die mathematischen Methoden der Theoretischen Physik, Vieweg, Braunschweig 1976.
16 V. Swaminathian, W. R. Wagner, P. J. Anthony, G. Henein and L. A. Koszi, J. Appl. Phys., 54 (1983) 7, 3763.
17 A. J. Yerman, J. F. Burgess, R. O. Carlson and C. A. Neugebauer, IEEE Trans. Compon., Hybrids, Manuf. Technol., 6 (1983) 473.

Zusammenfassung — Neue Ergebnisse von stationären 2-dimensionalen Temperaturberechnungen mittels *FEM* in Hochleistungslaserdiodenarrays werden vorgestellt. Der Einfluß verschiedener thermischer Lasten auf die Temperaturverteilung in AlGaAs/GaAs gewinngeführten Laserarrays wird untersucht. Das *FEM*-Modell wird mit einem analytischen Modell verglichen. Die mit diesen Modellen berechneten Maximaltemperaturen stimmen auf 1% überein. Der quatitative Einfluß verschiedener Größen (Verhältnis der emittierenden zu nichtemittierenden Gebieten, Joulesche Wärme, Stromspreizung, Lotschichten sowie nichtbenetzte Bereiche), die den thermischen Wiederstand des Bauelements beeinflussen, wird untersucht. Aus den Ergebnissen werden Regeln für einen optimalen thermischen Aufbau abgeleitet.